공학석사학위논문

Improving Detection Performance of Ionospheric Disturbances due to Earthquake with a Noise Reduction Method

잡음감소 미분법을 이용한 지진에 의한 전리층 교란 검출 성능 향상

2019년 2월

서울대학교 대학원

기계항공공학부

강 선 호

Abstract

Improving Detection Performance of Ionospheric Disturbances due to Earthquake with a Noise Reduction Method

Seonho Kang

School of Mechanical and Aerospace Engineering

The Graduate School

Seoul National University

Energy generated from earthquake is transferred to the ionosphere by earth-atmosphere coupling and results in co-seismic ionospheric disturbances (CID). CID can be observed in the ionospheric delay measurement using L1, L2 frequency carrier phase. As the diurnal change of ionospheric delay is generally larger than the disturbance, several methods are used to isolate the disturbance from normal ionospheric trends: band-pass filter, time derivative, etc. When using the derivative method, however, the disturbance signal can be obscured by measurement noise due to its small magnitude. This happens either because the earthquake is too small or the signal is too far from the epicenter. To effectively detect such weak disturbances from the noise, it is essential to increase the signal-to-noise ratio (SNR) of the disturbance.

In this paper, a new noise-reducing time derivative is suggested.

There are two assumptions. First, we assume that ionospheric delay changes smoothly; the ionospheric change is considered to be linear for the time span used in derivative. Second, ionospheric delay noise is regarded as Gaussian random. The designed sequential measurement combination was applied to 2011 Tohoku earthquake case. Its performance was compared with conventional de-trending methods including band-pass and time derivative. Performance index was chosen as the ratio of the absolute maximum value of disturbances to the standard deviation of normal ionospheric trend, which accounts for SNR.

Epicenter estimation was performed based on CID information. CID detection time was extracted using the proposed time derivative algorithm. A simple 2D wave propagation model was adopted for CID model. Epicenter estimation error was compared to that of previous study.

Keywords: Ionosphere, Co-seismic ionospheric disturbances, Earthquake, Signal-to-Noise Ratio, Epicenter

Student Number: 2017-24591

Contents

List of Figures

List of Tables

I. Introduction

1. Motivation and Objective

Energy generated by earthquake, volcanic eruption, etc., are transmitted to the atmosphere by energy coupling of the crust and the atmosphere [1, 2]. Sudden vertical displacement in the crust produces acoustic gravity waves [3], which move to the ionosphere and produce motion of neutral particles. Neutral particles in turn transmit the momentum to the electrons in the ionosphere and consequently disturb the electron density [2]. This disturbance is called Co-seismic Ionospheric Disturbances (CID) [4], which propagate as circular wave from the epicenter at ionospheric height.

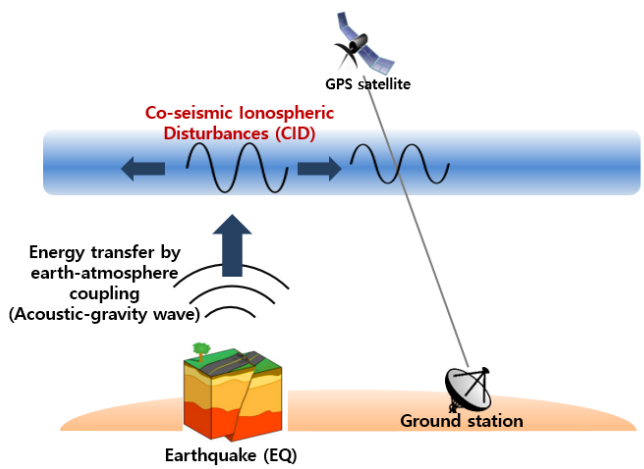

Figure I-1. CID detection by GPS signal

The signal of Global Navigation Satellite System (GNSS) changes speed as it passes through the ionosphere, where the rate of change varies with frequency. This can be used to estimate the Total Electron Content (TEC) on the satellite signal path using the dual frequency GNSS signal. Therefore, using the GNSS signal, it is possible to observe the ionospheric disturbance by ground sources such as earthquakes.

However, there are a couple of factors that attribute to small size of CID and incur poor detection performance. One factor is the small magnitude of earthquake. Generally, only earthquakes with a magnitude of 6.5 or higher are known to cause detectable disturbances in the ionosphere [5]. The other factor is signal's long distance from epicenter. Earthquake-induced ionospheric disturbances are reduced in size due to energy loss if the measured signal is far from the epicenter.

CID monitoring is very limited without improving the detection performance of small CID, which means that majority of CID data are left undetected. More specifically, as ground receivers for GPS are very constricted for its installation, CID by earthquakes in deep sea can only be detected with reduced amplitude. Also, if one wants to use domestic data for earthquake in distance as in this study, only small CID's are available for detection. Therefore, it is one of primary goals in this field of study to improve the detection performance of small CID, or increasing the Signal-to-Noise Ratio (SNR) of CID.

As an initial step for data processing, the normal trends in ionospheric delay signal need to be removed. Most commonly used

are band-pass filter and numerical derivative. In this study, we adopted numerical derivative for de-trending, as there are not much room for modification in band-pass filter algorithm.

We will design an algorithm to improve SNR of CID by reducing noise and preserving CID. We will also look at the effect of signal delay on the number of data used. The performance of the designed algorithm with the band-pass filter and the existing derivative methods will be compared.

The location of ground source is estimated using the initial CID detection time and location of the Ionospheric Pierce Point (IPP). The estimation algorithm performs iteration in the direction of minimizing the error for the CID propagation model. Epicenter estimation uses CID by Rayleigh wave. The energy caused by earthquakes proceeds with various waves such as Rayleigh wave and Acoustic-gravity wave. Here, CID by Rayleigh wave is observed earliest and biggest. This is because there is no disturbance until the arrival of CID by Rayleigh wave and it is generally larger than other types of CID.

CID by Rayleigh wave is known to propagate as a circular wave of 3.5 km/s [5, 7]. We will use this to in the CID propagation model and estimate the location of the epicenter that minimizes the error through an iterative process.

2. Trends of Research

The studies on the ionospheric disturbances due to earthquakes are mainly focused in phenomenon analysis. Most of them were performed using GNSS data at intervals of 30 seconds, and the band-pass results were main algorithm for detection. It is known that CID's energy is dominant at 3.7mHz and 4.4mHz [1]. In order to detect these energy, passbands including 1-10mHz [8], 1-8mHz [9], 0.5-5mHz [10] have been used in the previous studies.

There is a study on tsunami detection using time derivative of ionospheric disturbances. This method extracts the ionospheric disturbance signal by tsunami with a large frequency by increasing the interval of numerical derivative [11, 12]. In addition, there is a method of using the numerical 3rd derivative of data at intervals of 30 seconds [12, 13, 14]. Park et al. used this to analyze not only the earthquake but also the Underground Nuclear Explosion (UNE).

The overall trend in this field of study is phenomenon analysis, and there are no unified detection criteria or energy transfer model for CID due to its complex mechanism.

As for the epicenter estimation, there was a study on finding epicenter by estimating the center of a circular CID in time frame [16], Another study estimated the CID velocity and the ionospheric wind to improve estimation performance [15].

3. Research Contents and Method

In this paper, two studies were performed. The first is to improve the CID detection performance and the second is to improve epicenter estimation using CID.

The enhancement of CID detection was performed by increasing SNR of signal. By using time derivative as a de-trending method, we designed an algorithm that minimizes the noise of the differentiated results. We also analyzed what number of data epochs is appropriate in terms of SNR. In addition, SNR in real-time early detection scenario was analyzed. The performance of the designed algorithm is compared with band-pass filter, moving average filter, and moving average filter with expanded time step. In addition to simulation analysis, we analyzed the actual data of the 2011 Tohoku earthquake.

The epicenter estimation utilizes the disturbance detection time and the IPP position of the satellite signal at the disturbance detection point. Detection time of the disturbance is based on the result of the designed algorithm. The CID propagation model is assumed to be a two-dimensional constant velocity circular wave model. Finally, the result of epicenter was compared with the previous studies.

4. Contribution

In this paper, a new time derivative method was introduced, which improves CID detection performance. Minimum Noise Derivative (MND), the designed algorithm, minimizes noise under certain conditions. It turns out that the SNR of the CID is maximized when one epoch's time rate is estimated using 100 epochs. Compared with the moving average and band-pass results, 12% and 13% performance improvement was confirmed, respectively. Also, in case of TSMA (Time Step & Moving Average), which performs moving average with widened time interval of difference, MND and maximum SNR have the same performance. However, the SNR of MND is relatively higher when small epochs were used. This means that MND performance is superior to TSMA in terms of fast detection & early warning scenario.

In addition, we estimated the epicenter of 2011 Tohoku earthquake using the Korean GNSS stations. MND result was used to calculate the arrival time of CID, and the wave model assumed 2D propagation. The CID was presumed to move at a constant velocity of 3.5 km/s. Epicenter estimation using prn5, 15, 26, and 27 resulted in a position error of 91 km from the actual epicenter, 45% improvement over the previous study with an error of 170 km [16].

II. Ionospheric Disturbance Detection

In this chapter, we will look at how to estimate the Total Electron Content (TEC) of ionosphere using GPS signals and analyze conventional de-trending methods. Then we will suggest a new algorithm and compare the characteristics of each algorithm.

1. Ionospheric Combination of Carrier Phase

GPS signal provides pseudorange and carrier phase measurements. While satellite signals are transmitted from satellites to receivers, there are several error sources such ionosphere, troposphere, multi-path, etc. The ionospheric delay occurs when the speed of the satellite signal changes due to the electron density in the ionosphere. The ionospheric delay is known to be proportional to the total amount of electrons in the path of satellite signal. The following equation shows how TEC is calculated.

$$TEC = \int n_e(l)dl \qquad \text{(II.1)}$$

Here, $n_e(l)$ means electron density. The relationship between L1 ionospheric delay I_1 and TEC is like the following [17]. (f_1:

1575.42 MHz)

$$TEC = \frac{f_1^2}{40.3} I_1 \qquad \text{(II.2)}$$

In order to detect and analyze small-sized ionospheric anomalies, it is necessary to estimate the ionospheric delay using carrier phase measurement whose noise level is of several centimeters. There is ambiguity issue in carrier phase, but the bias error due to the ambiguity is not a problem in this study in which bias is illuminated by de-trending. The carrier phase L1 and L2 signals can be expressed as follows.

$$\begin{aligned} \phi_1 &= d + B - b - I_1 + T + \lambda_1 N_1 + \varepsilon_1 \\ \phi_2 &= d + B - b - \gamma I_1 + T + \lambda_2 N_2 + \varepsilon_2, \quad (\gamma = (\frac{f_1}{f_2})^2) \end{aligned} \qquad \text{(II.3)}$$

B is the receiver clock error, b is the satellite clock error, I is the ionospheric error, T is the tropospheric error, N is ambiguity, λ is wavelength of carrier phase, and ε is noise. The f_1 and f_2 used in γ calculation represent the L1 and L2 frequencies, respectively. If the two equations are linearly combined, we can make the ionosphere combination as shown below, where the ionosphere combination has three components: ionospheric delay,

bias, and noise.

$$\begin{aligned}\phi_{Iono} &= \frac{\phi_1 - \phi_2}{\gamma - 1} = I_1 + \frac{\lambda_1 N_1 - \lambda_2 N_2}{\gamma - 1} + \frac{\varepsilon_1 - \varepsilon_2}{\gamma - 1} \\ &= I_1 + bias + \varepsilon_{Iono}\end{aligned} \qquad (\text{II.4})$$

When ϕ_{Iono} is differentiated n times,

$$\phi_{Iono}^{(n)} = I_1^{(n)} + \varepsilon_1^{(n)} \qquad (\text{II.5})$$

As can be seen from the above equation, bias term is removed by the derivative, and consequently, only time derivative of ionospheric delay and noise remain.

2. Ionospheric Disturbance by Earthquake

Ionospheric disturbances due to earthquakes are largely classified into four types. First, when an earthquake occurs, the acoustic wave generated by the impact of epicentral surface moves to the ionosphere, causing disturbance. Since the acoustic wave at this time originates from the epicenter, its size decreases as it moves away from the epicenter. Acoustic waves have different velocity

distributions depending on the altitude, so they are refracted along with the progression. In the case of acoustic waves with low elevation angle, they are refracted back to the ground surface without reaching the ionosphere. This can be seen in Figure II-1. Ray-tracing of an acoustic wave that propagates under a certain degree of elevation can be confirmed to return to the ground surface by refraction. Also, it can be seen that acoustic waves starting at too high elevation angles pass through the ionosphere in the vertical direction. In short, acoustic waves that can propagate horizontally around the epicenter are very limited. As a result, only acoustic waves starting at an appropriate level of elevation can move horizontally, so that the disturbance of the ionosphere by the direct acoustic wave originating from the epicenter can be thought of as one acoustic wave rather than a superposition of waves.

In addition, when the acoustic wave moves in the gravitational field, the compressed gas has a higher density than the surrounding area, and therefore receives the force in the direction of the surface due to gravity. Conversely, the inflated gas having a lower density receives the buoyancy in the opposite direction. Thus, when an acoustic wave contains the characteristics of a gravity wave in a gravitational field with a gradient, it becomes an acoustic gravity wave (AGW) [18]. While pure acoustic waves have compressibility as restorative force and pure gravity waves have buoyancy as restoring force, AGW has both compression and buoyancy as resilience. Since the AGW velocity is similar to an acoustic wave, it is possible to estimate the time it takes to reach the ionosphere or

the speed of the AGW moving at a certain altitude using the acoustic wave speed according to the altitude.

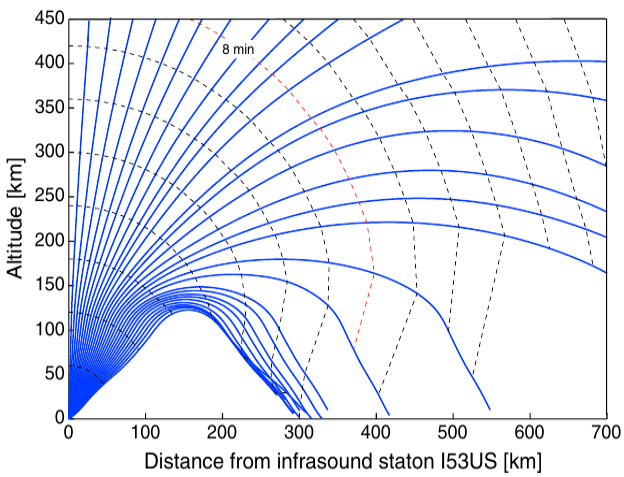

Figure II-1. Acoustic wave ray-tracing by point source (Yang, 2014 [17])

Secondly, it is the ionospheric gravity wave created by the energy applied to the ionosphere by the AGW just above the epicenter after the earthquake. Gravity waves are generated in the ionosphere by energy reaching the ionosphere. At this time, the gravity wave generated from the ionosphere is very similar to the surface wave generated from the water surface. Circular waves are repeatedly spread around the vertical center of the epicenter, and the size decreases as the distance from the epicenter increases.

Third, there is ionospheric disturbance by the Rayleigh wave, which is a surface wave moving around the epicenter when the

earthquake occurs. The Rayleigh wave travels from the ground to a circular wave with a speed of about 3.5 km/s. The feature of the ionospheric disturbance by the Rayleigh wave is that the horizontal velocity of 3.5 km/s, which is the Rayleigh wave velocity on the ground, is observed equally in the ionospheric disturbance. As the Rayleigh wave moves on the ground, the acoustic waves generated on the surface spread to the spherical wave around the surface where the displacement occurs. At this time, acoustic waves starting with low elevation angle with respect to the ground surface are refracted while moving and then return to the ground surface, and only acoustic waves starting at high elevation angles reach the ionosphere. Among them, the movement in the vertical direction has the shortest travel distance, so energy attenuation occurs to the minimum and reaches the ionosphere the earliest. Therefore, the effect of the acoustic wave generated by the Rayleigh wave and observed in the ionosphere can be attributed mostly to the energy propagated in the vertical direction. Hence, the disturbance of the same velocity is observed in the ionosphere after about 10 minutes, the time in which the acoustic wave travels from ground to ionosphere. As a result, the ionospheric disturbance by the Rayleigh wave appears to be caused by different acoustic waves arriving at the ionosphere sequentially. The velocity of the Rayleigh wave is the earliest because it is the fastest of the ionospheric disturbances caused by the earthquake.

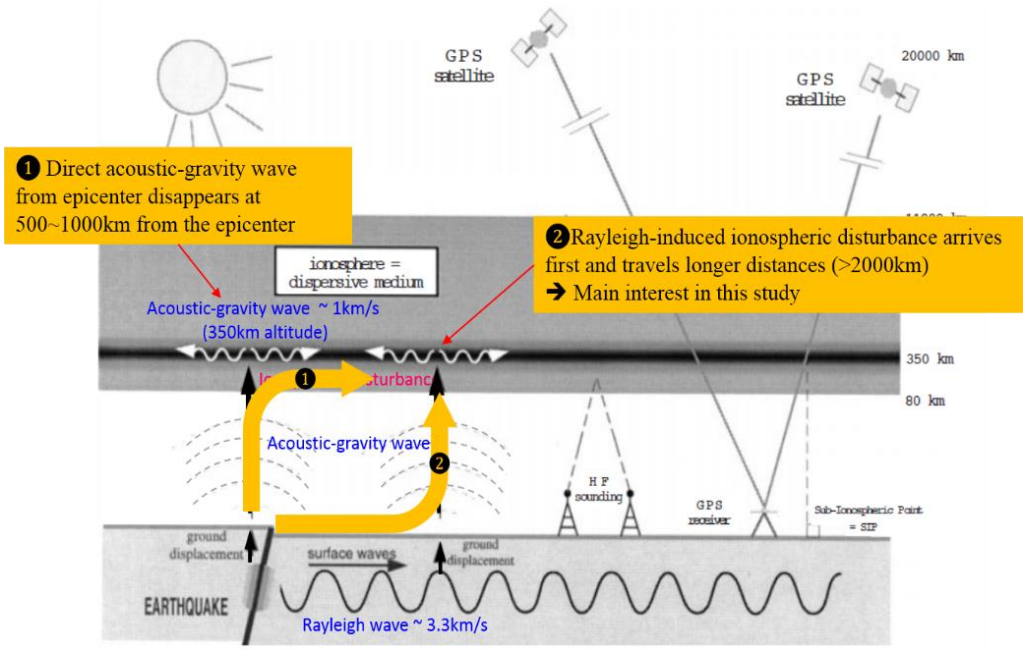

Figure II-2. Wave propagation by earthquake (Calais, 1995 [2])

Finally, when an earthquake occurs at sea, ionospheric disturbance by tsunami may occur. Since tsunami can assume a shallow water wave, the speed of tsunami can be calculated as $v_{tsunami} = \sqrt{gH}$. g is the gravitational acceleration, and H is the depth of water. The speed of tsunami in the sea of 6000 m depth is 243 m/s. The speed of a typical tsunami corresponds to 200 to 300 m/s. In the case of tsunami, the sea level gravity wave propagates into the atmosphere through the atmosphere and coupling process. At this time, tsunami is not a sudden movement to induce atmospheric compression, so the shape of the disturbance wave transmitted to the atmosphere is also a gravity wave. According to the previous study,

the ionospheric disturbance by tsunami at this time has the same speed as tsunami in the horizontal direction and 50 m/s in the vertical direction [9]. Because of these speed characteristics, ionospheric disturbance by tsunami has a unique property. First, when tsunami progresses in the water, energy from it has already the same horizontal and vertical velocity as tsunami, so that disturbance is not observed above the epicenter in a short time. At an average speed of 50 m/s, it takes 30 ~ 40 minutes to reach the ionosphere. During this time, the gravity wave has moved 400 to 500 km in the horizontal direction. Therefore, the ionospheric disturbance due to tsunami is not observed within a radius of 500 km on the basis of the epicenter, and even if it is observed, its size is small.

In addition, since it has the same speed as tsunami in the horizontal direction, if the disturbance due to tsunami is observed in the ionosphere, it can be confirmed that tsunami moves directly below. This is illustrated schematically in Figure II-3. The gravity wave arriving at the ionosphere just above the tsunami is the disturbance energy starting from sea level 30 ~ 40 minutes ago.

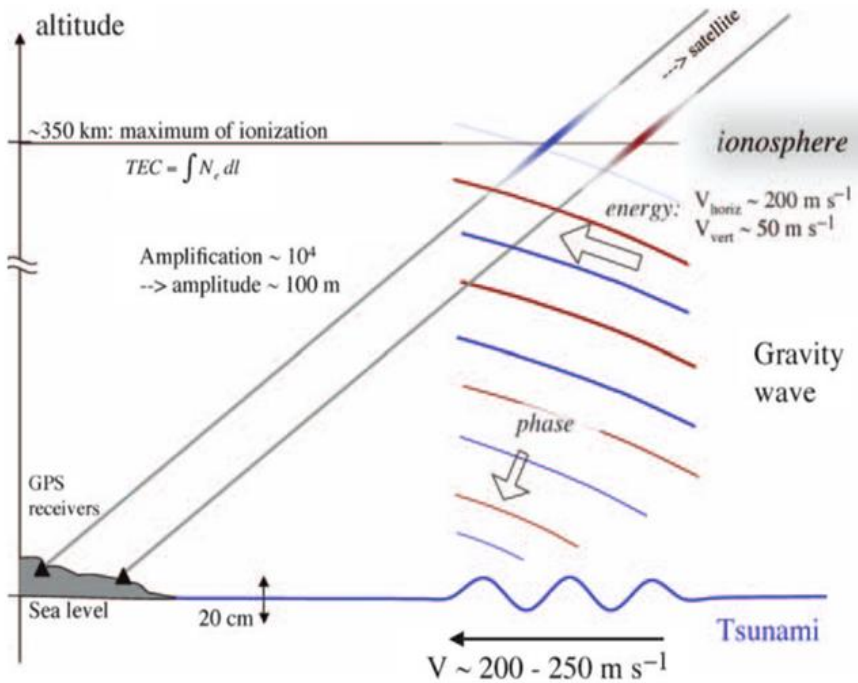

Figure II-3. Internal gravity wave by tsunami (Artru, 2004 [9])

Another feature of tsunami is that it is very small when it moves in the sea, not on the coast. As can be seen in Figure II-4, the tsunami in the deep sea has a wavelength of 100km or more, and a wave height of less than 1 m. This is one of the factors that makes tsunami detection in the deep sea very difficult. As can be seen in equation $v_{tsunami} = \sqrt{gH}$, the tsunami's velocity is large in deep sea and continually reduced on the way toward coast due to decreasing H . Decreasing speed of tsunami results in larger wave height as water accumulates on the coast, which causes damage. In deep sea, the tsunami is hard to detect due to its small amplitude. However, the

ionospheric disturbance due to tsunami can be observed because it has been amplified through rising to the atmosphere. This is due to the combination of exponentially decreasing air density and the conservation of energy. Finally, an approaching tsunami can be detected in advance at the low elevation using the GNSS reference station located on the coast. Tsunami's prediction is very important even if it's only a few minutes in advance, because many human and property damage can be prevented.

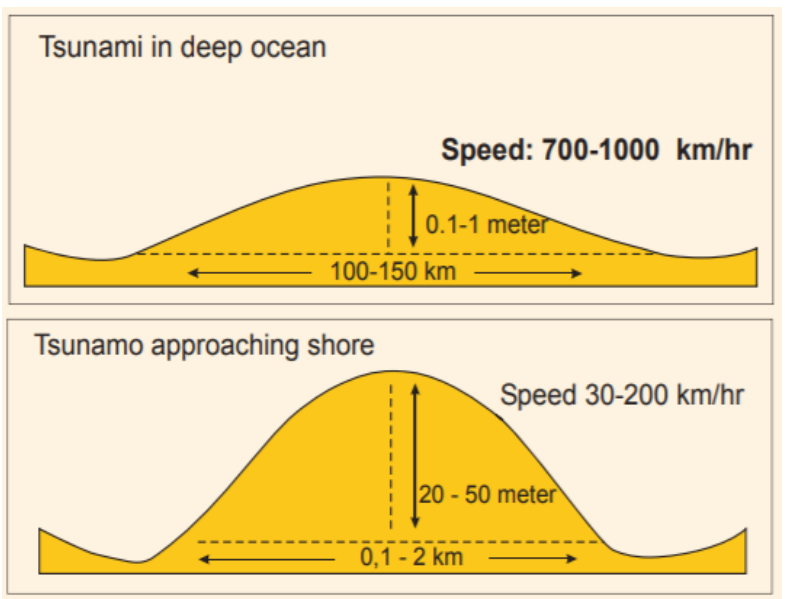

Figure II-4. Tsunami in deep sea and shore (ITC)

III. CID Detection Algorithms

In this section, we introduce conventional CID detection methods and propose a new detection algorithm that improves SNR of CID.

Ionospheric delay has normal trends due to several factors: diurnal change, seasonal change, geometry between the satellite and the receiver, and so on. As for diurnal change, the ionosphere has the largest electron density around 2 PM local time. Season also affects ionosphere and its electron density has semi-annual peaks around equinox. As to the geometry between the satellite and the receiver, ionospheric delay gets bigger with low elevation angle, as the path through the GNSS signal becomes longer. Even without earthquake and other events, there is trend in ionospheric delay, which needs to be removed for effective disturbance detection. If the ionospheric delay has a tendency, a reference value cannot be set for detection and the algorithm fails.

1. Band-pass Filtering

The de-trending by band-pass filtering is the most widely used method. Generally, the Butterworth method is used for its fast computation, and the passband is set to include the frequency of the ionospheric disturbance. There are various opinions about which passband is better to set, but usually frequency band between 1-

10mHz is used. The result of the band-pass filter is the meter itself because it de-trends the ionospheric delay value itself. In the case of the band-pass filter, there are many factors to consider, such as computation burden exponentially increasing with precision level, an edge effect at both ends of the signal to be processed, and vulnerability to abnormal data such as NaN.

2. Numerical 3rd Order Derivative

In the previous research, numerical 3rd order derivative using 30-second data was used to eliminate the tendency [14]. The formula is shown in . . s_i means the ionosphere combination value in the i^{th} epoch, which is calculated by linear combination of L1 and L2 carrier phases. It can be seen that there is a difference between the differential form and the numerical derivative such as the forward difference and the central difference which are generally used. The type of time derivative used in the previous study is as follows. Since we use 3 epochs to perform the difference, we can see that the first and last epoch of the whole data is reduced each time a differentiation is made. Here Δt equals $2(t_i - t_{i-1})$.

Numerical derivative is different from the general numerical differentiation, so we need to look at the formula for intuitive understanding. Equation ((III.3) is the relationship between the numerical 3rd derivative and the general forward difference.

Numerical derivatives are denoted by $s^{'}$, and general forward differences denoted by $\dot{s}$.

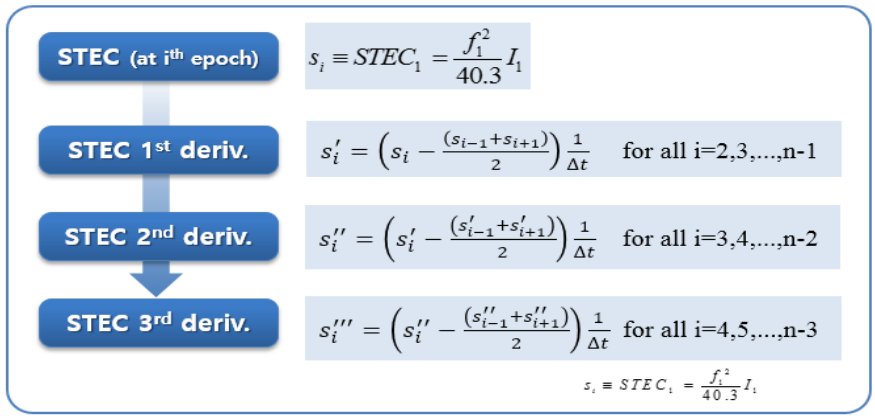

Figure III-1. Numerical 3rd order derivative [14]

$$
\begin{aligned}
s_i^{'} &= (s_i - \frac{s_{i-1}+s_{i+1}}{2})\frac{1}{\Delta t} \\
&= -\frac{1}{4}(\frac{s_{i+1}-s_i}{\Delta t/2} - \frac{s_i - s_{i-1}}{\Delta t/2}) \\
&= -\frac{1}{4}(\dot{s}_i - \dot{s}_{i-1}) \\
&= -\frac{\Delta t}{8}(\frac{\dot{s}_i - \dot{s}_{i-1}}{\Delta t/2}) \\
&= -\frac{\Delta t}{8}\ddot{s}_{i-1}
\end{aligned}
\qquad \text{(III.1)}
$$

$$s_i'' = \frac{(\Delta t)^2}{8^2} s_{i-2}^{(4)} \qquad (\text{III.2})$$

$$s_i''' = \frac{(\Delta t)^3}{8^3} s_{i-3}^{(6)} \qquad (\text{III.3})$$

As can be seen in Figure III−1, the numerical 3rd order used in the previous study is the same as multiplying the sixth order forward difference by a constant. Since the difference has the effect of a high−pass filter that reduces trend in the low frequency region, it can be expected that the tendency of the diurnal change, seasonal change, and geometry can be eliminated.

3. Forward Difference & Moving Average

In section [III−3] to [III−5], we will derive algorithms that improve SNR of CID detection by combination of sequential measurements. Unlike the previous studies, here we will investigate ways to reduce noise by properly adjusting the combination coefficients for numerical differentiation, will consequently increase the SNR of CID.

Before elaborating on the algorithms, there are two assumptions that we adopted to estimate time rate and calculate the noise level as shown in Table III−1.

Table III−1. Two assumptions for derivative methods

No.	Comment
1	Ionosphere delay changes linearly over a short time
2	The noise of the ionosphere delay is Random Gaussian

The first assumption is that the ionosphere delay changes linearly over a short time. Tendency in ionospheric delay due to diurnal changes has a period of several hours. Also, according to previous studies, the initial disturbance of CID has a frequency of 4.4 mHz or a period of 225 sec for the Rayleigh wave [19]. Therefore, we can see that the ionosphere delay is close to linear for 100 sec, as can be seen in Figure III−2. This assumption is then used to replace the second and higher terms with zero in the Taylor expansion.

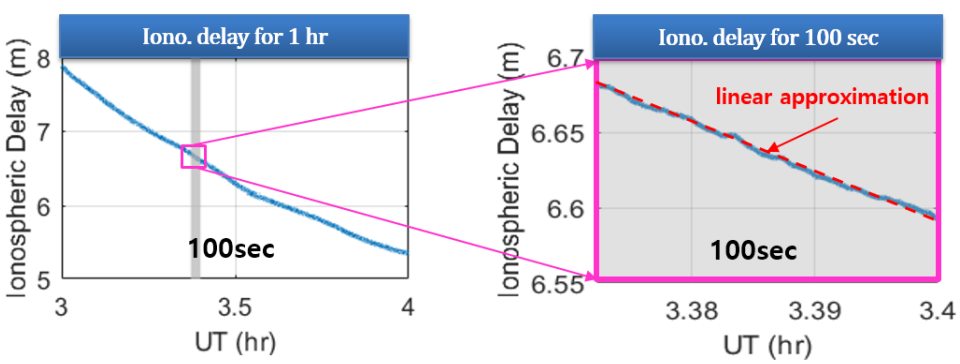

Figure III−2. Linearity of ionospheric delay over a short time

The second assumption is that the noise of the ionosphere delay is a random Gaussian noise. This is a common assumption for noise. As a result, ionospheric combination measurements can be expressed as the sum of normal trend, CID, and Gaussian noise.

One of the first ways to reduce the noise of differential results is to apply a basic noise reduction to the basic differential. The most basic derivative is forward difference that subtracts the sequential data, and the commonly used noise reduction method is the moving average. Here, we will call it Forward difference & moving average, or FDMA. Using both together, applying the moving average to the forward difference result can be expressed as Figure III-3.

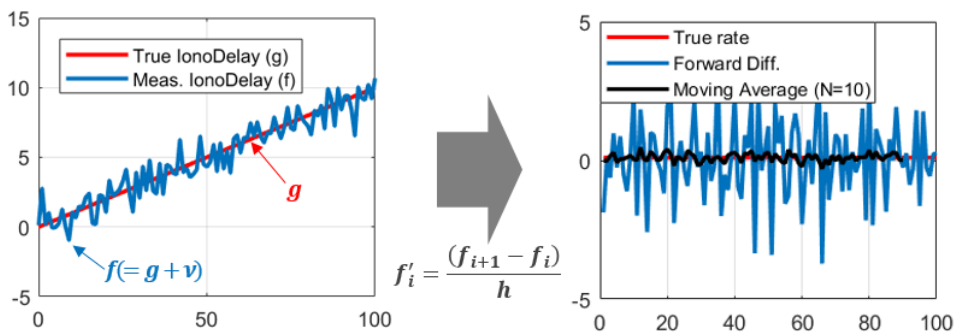

Figure III-3. Forward difference & moving average

If we denote ionospheric delay as g, ionospheric combination as f, and noise as v, the following equation holds. Each epoch in f is estimated to be an ionosphere combination.

$$f = g + \nu \qquad \text{(III.4)}$$

In order to de-trend ionospheric combination, forward difference can be used as in Equation (III.5).

$$f_i^{'} = \frac{f_{i+1} - f_i}{h} \qquad \text{(III.5)}$$

The most common way to reduce noise in data with a certain signal is to use moving average. If we apply moving average to the result of forward difference, It can be denoted as Equation (III.6). Here, $h = 1(\sec)$ as only 1-sec interval data is used in this paper.

$$\begin{aligned} f_1^{'} &= f_2 - f_1 \\ f_2^{'} &= f_3 - f_2 \\ &\vdots \\ f_{N-1}^{'} &= f_N - f_{N-1} \end{aligned} \qquad \text{(III.6)}$$

If all the terms are added, to the middle value $f_m = [m/2]$,

$$
\begin{aligned}
f_m^{'} &= \frac{f_1^{'} + f_2^{'} + \cdots f_{N-1}^{'}}{N-1} \\
&= \frac{f_N - f_1}{N-1} \\
&= \frac{g_N - g_1}{N-1} + \frac{\nu_N - \nu_1}{N-1} \\
&= \quad g_m^{'} \quad + \quad \nu_m^{'}
\end{aligned}
\qquad \text{(III.7)}
$$

Here, $\nu_m^{'}$ is the noise part in ionospheric combination with $\nu \sim N(0, \sigma_\nu^2)$. The noise level of FDMA can be calculated as Equation (III.8).

$$
\begin{aligned}
\sigma_{\nu^{'}} &= \frac{\sqrt{1^2 + (-1)^2}}{N-1}\sigma_\nu \\
&= \frac{\sqrt{2}}{N-1}\sigma_\nu
\end{aligned}
\qquad \text{(III.8)}
$$

Therefore, the moving average is inversely proportional to the number of epochs used. Moving average, however, is not an algorithm that minimizes noise for correlated data. As there occurs correlation in the differenced data, moving average cannot confirm minimum noise level and there remains room for improvement in terms of noise.

4. Time Step & Moving Average

In case of forward difference & moving average, since it simply difference sequential data, there remain considerable noise in differential result. Noise can be further reduced by increasing the time interval of the derivative. This approach was adopted by a previous study by Zhang [11], which was used for detecting ionospheric disturbances by tsunami. In this paper, we combined derivative using expanded time step with moving average method, which we will call as Time step & moving average, or TSMA. This can be illustrated as Figure III−4.

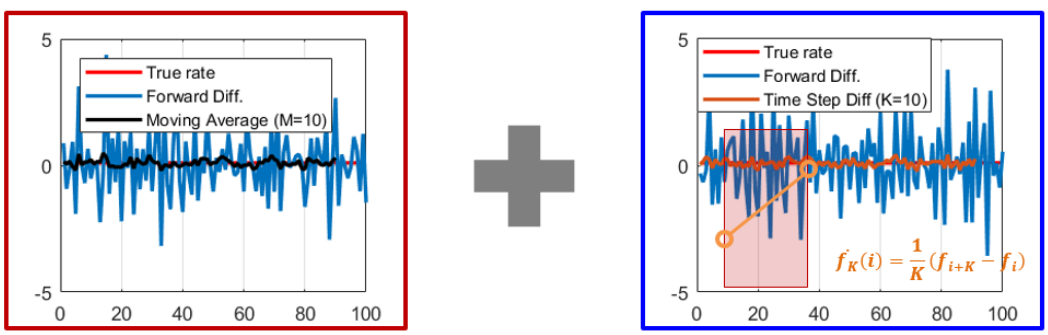

Figure III−4. Time step & moving average

Forward difference with expanded time step can be expressed as Equation (III.9).

$$\dot{f}_K(i) = \frac{1}{K}(f_{i+K} - f_i) \qquad \text{(III.9)}$$

Here K means time interval used for difference. If we apply moving average to this,

$$\begin{aligned}\dot{f}_{K,M}(i) &= \frac{1}{M}[\dot{f}_K(i) + \dot{f}_K(i+1) + \cdots + \dot{f}_K(i+M-1)] \\ &= \frac{1}{M}[\frac{1}{K}(f_{i+K} - f_i) + \cdots + \frac{1}{K}(f_{i+K+M-1} - f_{i+M-1})] \\ &= \frac{1}{KM}[-(f_i + \cdots + f_{i+M-1}) + (f_{i+K} + \cdots + f_{i+K+M-1})]\end{aligned} \qquad \text{(III.10)}$$

As can be seen in Equation (III.10), the total length of data epochs used is $N(i \le n \le i+K+M-1) = K+M$. In order to set the same length for derivative with other methods, we can set $N = K+M$, or $M = N-K$. Then Equation (III.10) turns to,

$$\begin{aligned}\dot{f}_K(i) &= \frac{1}{KM}[-(f_i + \cdots + f_{i+M-1}) + (f_{i+K} + \cdots + f_{i+K+M-1})] \\ &= \frac{1}{K(N-K)}[-(f_i + \cdots + f_{i+N-K-1}) + (f_{i+K} + \cdots + f_{i+N-1})]\end{aligned} \qquad \text{(III.11)}$$

If we derive the output of Equation (III.11) and find out regularity for different K's, $\dot{f}_K(i)$ for general K can be expressed

as Equation (III.12).

$$\begin{aligned}\dot{f}_K(i) &= \frac{1}{K(N-K)}[-(f_i+\cdots+f_{i+K})+(f_{i+N-K}+\cdots+f_{i+N-1})] \\ &= \frac{1}{K(N-K)}[-(g_i+\cdots+g_{i+K})+(g_{i+N-K}+\cdots+g_{i+N-1})] \\ &+ \frac{1}{K(N-K)}[-(\nu_i+\cdots+\nu_{i+K})+(\nu_{i+N-K}+\cdots+\nu_{i+N-1})]\end{aligned} \quad (\text{III.12})$$

In Equation (III.12), the noise level can be calculated using the coefficients of ν. As noise is assumed to be Gaussian random, the noise level is as followings.

$$\sigma_{\dot{\nu}} = \frac{\sqrt{2K}}{K(N-K)}\sigma_{\nu} \quad (\text{III.13})$$

Now, in order to derive the optimal ratio of K and M in $N = K + M$, gradient of noise level is calculated as in Equation (III.14).

$$\frac{\partial \sigma_{\dot{\nu}}}{\partial K} = \sigma_{\nu} \frac{\partial}{\partial K}[\frac{\sqrt{2K}}{K(N-K)}]$$
$$= \sigma_{\nu} \frac{3K-N}{K\sqrt{2K}(N-K)^2} \qquad \text{(III.14)}$$
$$\therefore K = \frac{N}{3}, \quad M = \frac{2N}{3}$$

In this case, solution and noise level are like the followings.

$$\dot{f}_N(i) = \frac{9}{2N^2}[-(f_i + \cdots + f_{i+\frac{N}{3}-1}) + (f_{i+\frac{2N}{3}-1} + \cdots + f_{i+N-1})] \qquad \text{(III.15)}$$

$$\sigma_{\dot{\nu}} = \frac{3\sqrt{6}}{2N\sqrt{N}}\sigma_{\nu} \qquad \text{(III.16)}$$

The noise level of FDMA is inversely proportional to N, while it is inversely proportional to $N^{1.5}$ in TSMA. Therefore, TSMA is superior to FDMA in terms of noise. However, TSMA is an algorithm that applies a moving average to data that has a correlation due to a derivative, as in FDMA. Therefore, its noise level still leaves room for improvement.

In the next section, we suggest a derivative algorithm that minimize noise level with a certain N.

5. Minimum Noise Derivative (Proposed)

To derive the optimal sequential combination to minimize noise, measurement needs to be expressed in Taylor expansion form.

$$\begin{aligned} f_{i+1} &= f_i + f_i^{'} + \frac{1}{2!} f_i^{''} + \cdots \\ f_{i+2} &= f_i + 2 f_i^{'} + \frac{2}{2!} f_i^{''} + \cdots \\ &\vdots \\ f_{i+N-1} &= f_i + (N-1) f_i^{'} + \frac{N}{2!} f_i^{''} + \cdots \end{aligned} \qquad \text{(III.17)}$$

Applying the first assumption of ionospheric linear rate of change, we can replace the second and higher order terms with zero. Then, for linear combination, multiply each term by arbitrary coefficients $a_1, a_2, \cdots, a_{N-1}$, and it can be expressed as Equation (III.18).

$$\begin{aligned} a_1 f_{i+1} &= a_1 f_i + a_1 f_i^{'} \\ a_2 f_{i+2} &= a_2 f_i + 2a_2 f_i^{'} \\ &\vdots \\ a_{N-1} f_{i+N-1} &= a_{N-1} f_i + a_{N-1}(N-1) f_i^{'} \end{aligned} \qquad \text{(III.18)}$$

In terms of $f_i^{'}$,

$$f_i^{'} = \frac{(-\sum_{j=1}^{N-1} a_j) f_i + \sum_{j=1}^{N-1} a_j f_{i+j}}{(a_1 + 2a_2 + \cdots + (N-1)a_{N-1})}$$

$$\begin{aligned} &= c_1 f_i + c_2 f_{i+1} + \cdots + c_N f_{i+N-1} \\ &= c_1 g_i + c_2 g_{i+1} + \cdots + c_N g_{i+N-1} \\ &\quad + c_1 f_i + c_2 f_{i+1} + \cdots + c_N f_{i+N-1} \\ &= g_i^{'} + \nu_i^{'} \end{aligned} \qquad \text{(III.19)}$$

As $\nu \sim N(0, \sigma_\nu^2)$, we can get minimum noise $\nu_i^{'}$ by setting the following objective.

$$\min_{a_1,\ldots,a_{N-1}} (c_1^2 + c_2^2 + \cdots + c_N^2) = \min_{a_1,\ldots,a_{N-1}} \frac{(\sum_{j=1}^{N-1} a_j)^2 + \sum_{j=1}^{N-1} a_j^2}{(\sum_{j=1}^{N-1} j a_j)^2} \qquad \text{(III.20)}$$

We need to find coefficients that minimizes the above cost. However, if you look at the cost, you can see that the same equation holds even if you divide the denominator and the numerator by a_1 respectively. Therefore, we adopted a pivot through setting $a_1 = 1$.

Next, we derive the coefficients using the property that the gradient becomes zero when cost has the minimum value.

$$J = \frac{(\sum_{j=1}^{N-1} a_j)^2 + \sum_{j=1}^{N-1} a_j^2}{(\sum_{j=1}^{N-1} j a_j)^2} = \frac{N}{D^2} \qquad \text{(III.21)}$$

$$\frac{\partial J}{\partial a_i} = 0 = \frac{D^2 \frac{\partial N}{\partial a_i} - 2ND \frac{\partial D}{\partial a_i}}{D^4} \qquad \text{(III.22)}$$
$$\therefore D \frac{\partial N}{\partial a_i} = 2N \frac{\partial D}{\partial a_i}$$

Here,

$$\begin{aligned} \frac{\partial N}{\partial a_i} &= \frac{\partial}{\partial a_i}[(a_1 + \cdots + a_{N-1})^2 + (a_1^2 + a_{N-1}^2)] \\ &= 2(\sum_{j=1}^{N-1} a_j + a_i) \\ \frac{\partial D}{\partial a_i} &= \frac{\partial}{\partial a_i}[a_1 + 2a_2 + \cdots + (N-1)a_{N-1}] \\ &= i \end{aligned} \qquad \text{(III.23)}$$

Therefore, if we combine Equation(III.22) and (III.23) together,

$$\frac{\sum_{j=1}^{N-1} a_j + a_i}{i} = \frac{N}{D} = const. \quad (i = 1,2,...,N-1) \qquad \text{(III.24)}$$

Then, Equation (III.24) implies $(N-2)$ equations as shown in Equation

$$\frac{\sum_{j=1}^{N-1} a_j + a_1}{1} = \frac{\sum_{j=1}^{N-1} a_j + a_i}{i} \quad (i = 2,...,N-1) \qquad \text{(III.25)}$$

There are $(N-1)$ unknowns in total, $a_1, a_2, ..., a_{N-1}$, and with the pivot $a_1 = 1$, and $(N-2)$ equations above the whole unknowns are solvable. The solution is expressed in Equation (III.26)

$$f_i^{'} = c_1 f_i + c_2 f_{i+1} + \cdots + c_N f_{i+N-1}$$
$$where, \; c_k = \frac{6[-(N-1) + 2(k-1)]}{(N-1)N(N+1)} \quad (k = 1,2,...,N) \qquad \text{(III.26)}$$

Also, we will call this derivative as Minimum Noise Derivative, or MND. The noise level of MND is shown in Equation (III.27),

$$\sigma_{\nu'} = \sqrt{\frac{12}{(N-1)N(N+1)}}\sigma_{\nu} \qquad \text{(III.27)}$$

6. Noise Level Comparison

Among five detection methods introduced, band-pass filter's noise level is not appropriate to formulate, as this filter heavily relies on data itself. Also, as the numerical 3rd order derivative is based on 30-sec interval data, it is not a proper comparison to analyze its noise level in respect to 1-sec interval data. Therefore, here we will compare the noise level of FDMA, TSMA, and MND. We used pure Gaussian random noise with length 10^5 and calculated standard deviation for different N s.

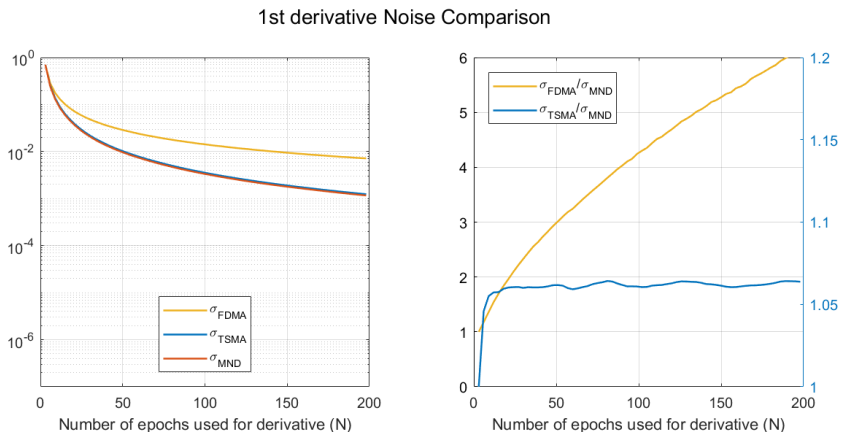

Figure III-5. Noise comparison of the first derivative

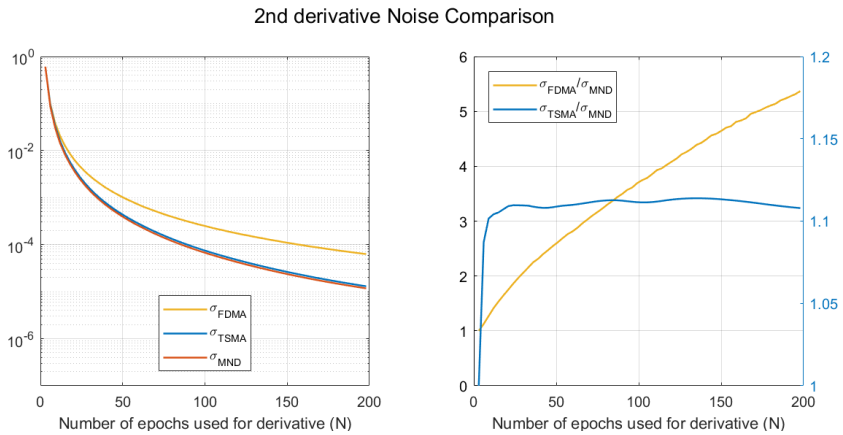

Figure III-6. Noise comparison of the second derivative

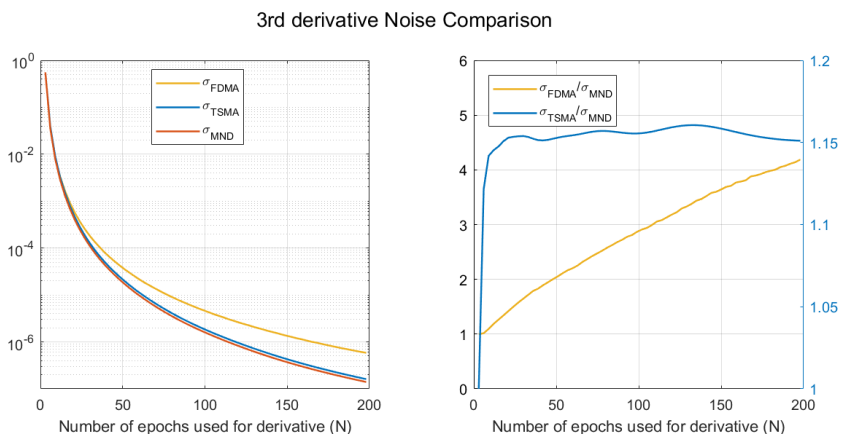

Figure III-7. Noise comparison of the third derivative

As shown in Figure III-5 to Figure III-7, MND and TSMA has much improved noise level compared to FDMA. This is predictable by σ_{ν}, calculated in the previous chapter, with Equation (III.8), (III.16), and (III.27).

For TSMA and MND comparison, it turns out that MND has 6%, 12%, and 15% improved noise level for 1st, 2nd, and 3rd derivative, respectively.

As for the derivative level, the gap between MND's and TSMA's noise level diverge as more differential was applied. However, FDMA showed gradually smaller gap with MND as derivative level increased. This can be attributed to the fact that FDMA has the least correlation and therefore its noise-reducing effect is well maintained.

Ⅳ.Performance of Detection Algorithms

In this chapter, we will analyze the performance of detection algorithms with respect to two aspects: maximum SNR, and SNR in early detection case. In Maximum SNR part, we will find out the best N associated with the maximum SNR for each algorithm and compare their performance. Next, SNR in early detection case will be analyzed, which in this case is a real-time application. For SNR calculation, real data of 2011 Tohoku Earthquake will be used.

1. The Tohoku Earthquake in 2011

At 05:46:24 UT on March 11, 2011, the massive Tohoku Earthquake occurred off the Pacific Coast of Japan's Sanriku region. The magnitude of the Richter scale was 9.1, and the location of the epicenter was latitude 38.297 deg and longitude 142.373 deg (USGS). Figure III-8 is an IPP near the epic of the GPS satellite for Korea's ANHN. The IPP shows the trajectory for 1 hour from immediately after the earthquake. The red dot indicates the position of the epicenter, and the purple triangle indicates the position of the ANHN station. On the line representing the IPP trajectory, one end indicated by an O indicates the time when the earthquake occurred, and the other end indicated by X represents the IPP position after 1 hour. From the figure, it appears that prn5 and prn26 are close to the epicenter at the time of the earthquake.

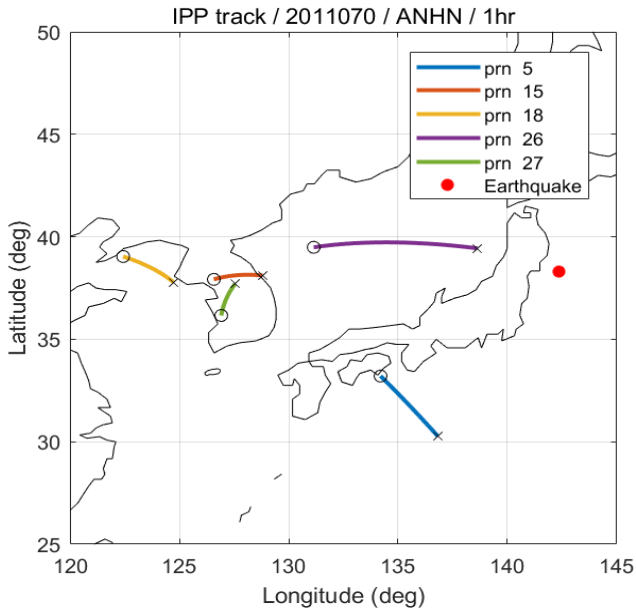

Figure III-8. IPP trajectory for 1 hour since earthquake (ANHN)

2. Monitoring Value

(1) Derivative Level

Even though there are viable options for CID detections, there are a couple of things to consider. The first is how many time difference to take when de-trending ionospheric combination. Here in this paper, we used the 3rd order derivative as in the previous study [14]. For the 3rd order derivative, normal trend in the ionospheric

combination is safely removed. To confirm this, we checked whether normal trend is removed in the 3rd order derivative with real data. For conservative confirmation, data of vernal equinox in solar maximum, where ionosphere activity was at its peak was used. As shown in Figure III-9, the ionospheric combination has its remaining trend until with the 2nd order derivative. However, with the 3rd order derivative, the normal trend is totally erased and only pure noise is to be seen. Therefore, we will use the 3rd order derivative of ionospheric combination.

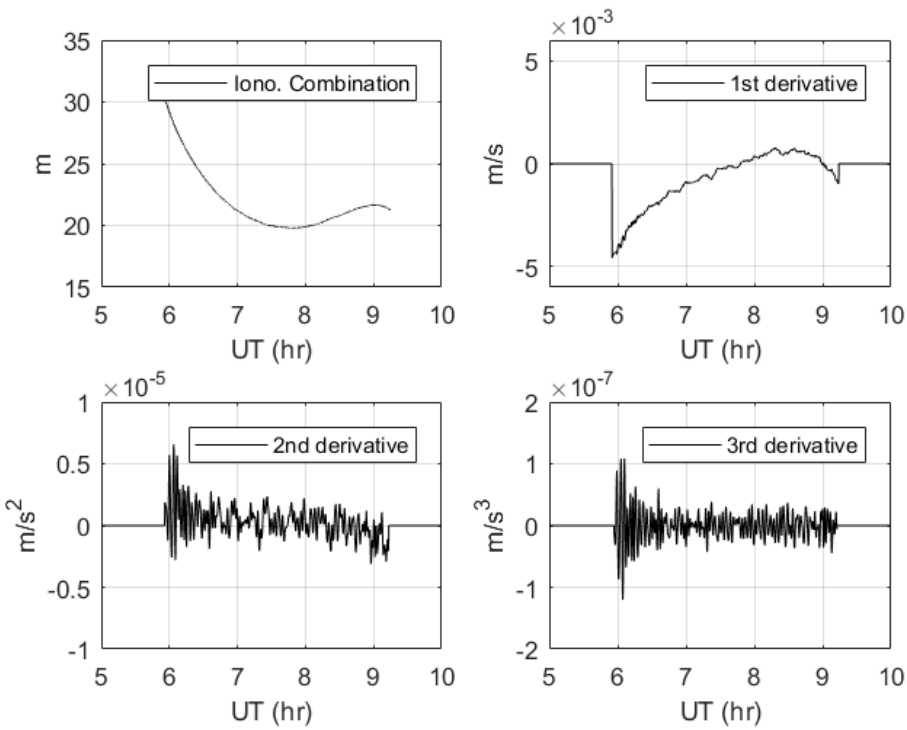

Figure III-9. MND derivatives of ionospheric combination with N=100 (2002079 usud)

(2) Number of Epochs for Derivative

Along with the derivative level, the number of epochs for derivative, or N should be determined for monitoring value of FDMA, TSMA, and MND. As the shape of disturbance is not stereotyped, we numerically calculated SNR for different N s. Here 45 stations of NGII (National Geographic Information Institute) in Korea and prn 15, 26, 27 were used. Figure III-10 shows an example of MND 3rd derivative of ionospheric combination.

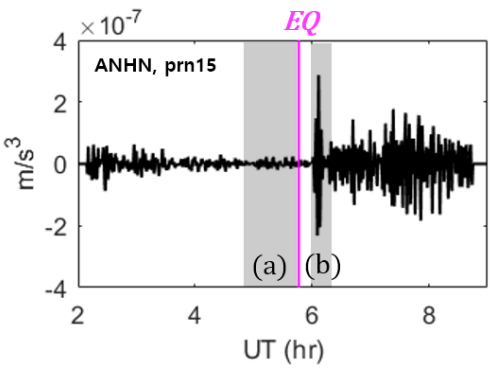

Figure III-10. Example of MND 3rd derivative of ionospheric combination (ANHN, prn 15)

As CID by Rayleigh wave has a short disturbance signal lasting several minutes, which varies data to data, conventional SNR may not be applicable to CID. Therefore, in this study we define SNR as Equation (III.28).

$$SNR = \frac{\max(|CID|)}{STD(noise)} \qquad \text{(III.28)}$$

$\max(|CID|)$ means the maximum of absolute CID measurements. This value is extracted from 10 min to 30 min after earthquake, where CID by Rayleigh wave is expected to arrive at 0 km to 2000 km from epicenter. $STD(noise)$ means the standard deviation of data without CID. This value is calculated from 1 hr before earthquake to the time of earthquake outbreak, which affirms there is no CID in the data at the same time minimizing the effect of elevation angle on noise. Time region of $STD(noise)$ and $\max(|CID|)$ are represented as shaded regions (a) and (b) respectively.

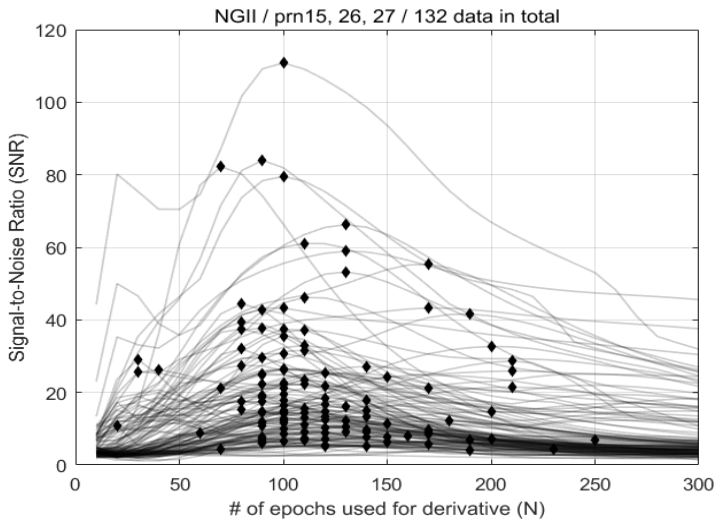

Figure III-11. MND's SNR by N for real data (2011 Tohoku Earthquake)

Figure III−11 shows SNR by N for 132 real data measurements of 2011 Tohoku Earthquake. In the figure each diamond refers to maximum SNR point. It turns out SNR is maximized around $N=100$ value. The number of maximum SNR points is shown in Figure III−12.

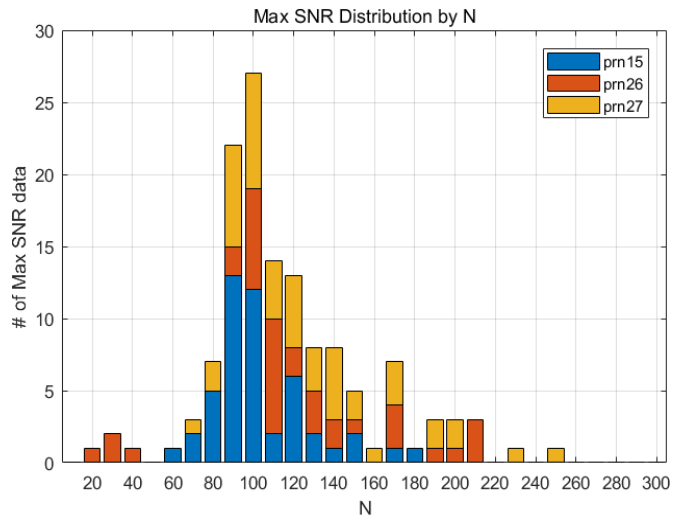

Figure III−12. MND's maximum SNR accumulation by N

It appears clear that $N=100$ is the best option for maximizing SNR for overall data for MND 3rd derivative. Same approach is applicable to FDMA and TSMA, which is shown in Figure III−13 and Figure III−14.

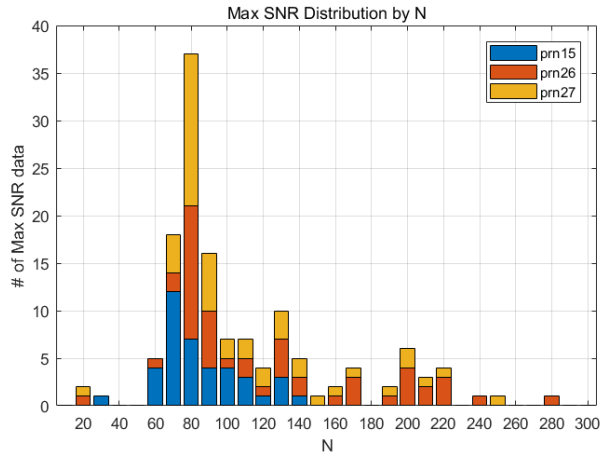

Figure III-13. FDMA's maximum SNR accumulation by N

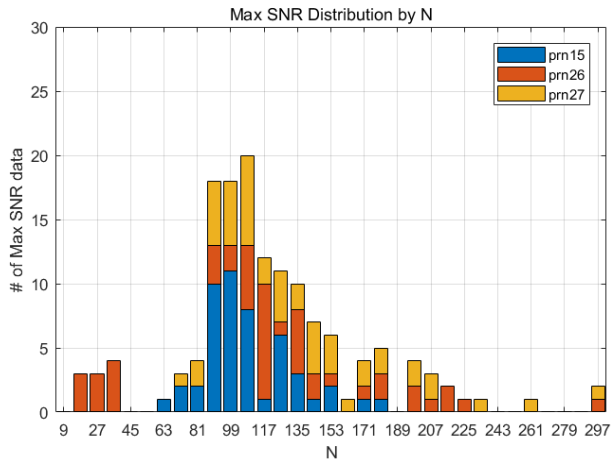

Figure III-14. TSMA's maximum SNR accumulation by N

Table III-2 shows best N's that maximize SNR for each algorithm. MND and FDMA's interval of N was set to be 10 and TSMA's 9. This difference is due to the fact that TSMA requires multiples of 3 for it optimality.

Table III-2. Best N's for MND, FDMA, and TSMA

Time Derivative	Best N
MND 3rd	100
FDMA 3rd	80
TSMA 3rd	108

3. Maximum SNR

With real data of Tohoku Earthquake in 2011, maximum SNR is compared for five detection algorithms. For band-pass algorithm, 3-20 mHz passband was chosen for detection, which include main energy concentrated in 3~5 mHz and at the same time reduce noise. This passband was chosen by trial and error, as analytic approach is not viable for band-pass filter.

Figure III-15 shows an example of filtering output for five detection algorithms introduced in this paper. As can be inferred from the figure, each algorithm has difference performance for different data measurements. Therefore, to compare SNR performance, we need to investigate the average values.

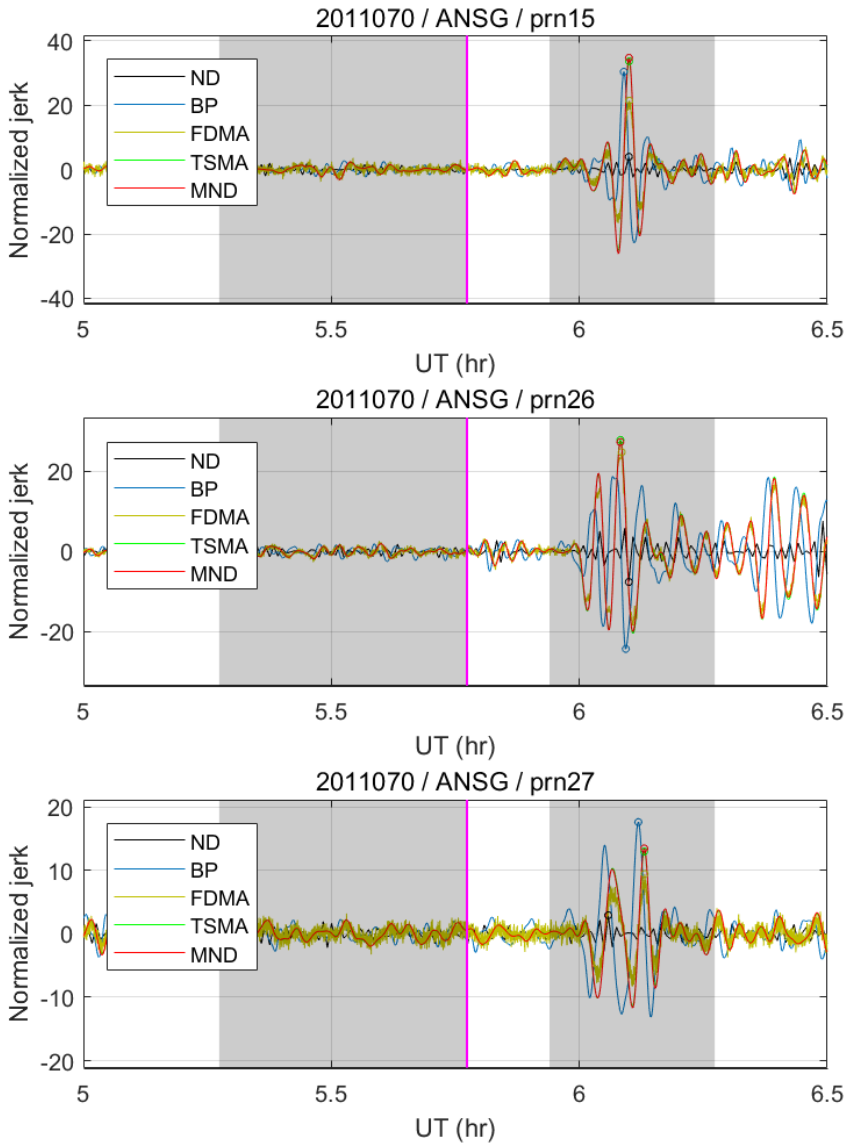

Figure III-15. Filtering output of five detection algorithms

Table III-3 shows the average values of maximum SNR for 45 NGII stations in Korea. As represented in Equation (III.28), these values are ratio of absolute maximum of CID to noise STD. Therefore,

if SNR is smaller than 3, it means disturbance signal is smaller than 3σ value of noise, which is practically undetectable. For Numerical 3rd order derivative, prn15 and 27 is not detectable on average, while prn26 is clearly detectable. Other detections show similar output, with prn26's average SNR the biggest and prn27's smallest. This is due to different distances to epicenter at the time of CID detection.

On the right side of the table is MND's improvement from other detection methods, which is average values for all data. MND showed over 300% improved result from Numerical 3rd order derivative, 12~13 % from band-pass and FDMA, -1 % from TSMA. Though TSMA showed a little higher performance, its difference is minor and thus it can be said that TSMA's and MND's maximum SNRs are of same levels.

Table III-3. Maximum SNR for five detection algorithms

Algorithm	prn15	prn26	prn27	Improvement of MND
Numerical 3rd (ND, 30-sec)	3.20	8.92	2.25	340.6 %
Band-pass (BP, 3-20 mHz)	16.65	20.08	8.05	13.6 %
FDMA 3rd	14.27	28.40	6.88	12.5 %
TSMA 3rd	17.71	29.37	7.95	-0.8 %
MND 3rd	17.87	28.98	7.89	-

4. SNR in Early Detection Case

Even though maximum SNR is of main interest for post processing of data, there is different consideration in real-time application. As detection algorithms use a certain length of data before and after the epoch of interest, it uses both past and future data with respect to the specific time. Since in real-time the future data is still to be measured, there occurs the time lag which is equal to half of N. Larger N, accordingly, means more time to detect CID for the same event.

There are real-time scenarios that require small time lag such as tsunami detection and early warning. In these scenarios, it is important to compare SNR performance in small N regions, where time lag is small as well. That is, SNR comparison in small N regions refers to performance analysis for early detection case.

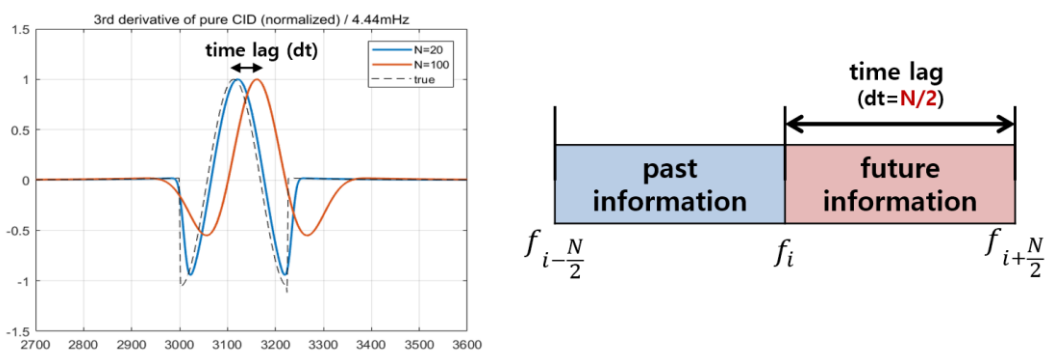

Figure III-16. Time lag of detection algorithms for real-time application

Left plot in Figure III−17 shows SNR by N of TSMA and MND. It can be inferred from the graph that MND's SNR graph is slightly located leftward compared to TSMA. MNS's SNR improvement from TSMA is on the right plot. As for the small N regions, we selected N regions from where SNR of TSMA exceeds 5 to where its value is at its peak. This region is represented as shades in Figure III−17. As can be inferred from the right plot, MND has better performance in small N regions.

Table III−4 shows average values of MND's improvement from TSMA in small N regions for 45 NGII stations in Korea. It turns out that MND has 6~7 % improvement from TSMA for maximum improvement and 3~4 % for mean improvement.

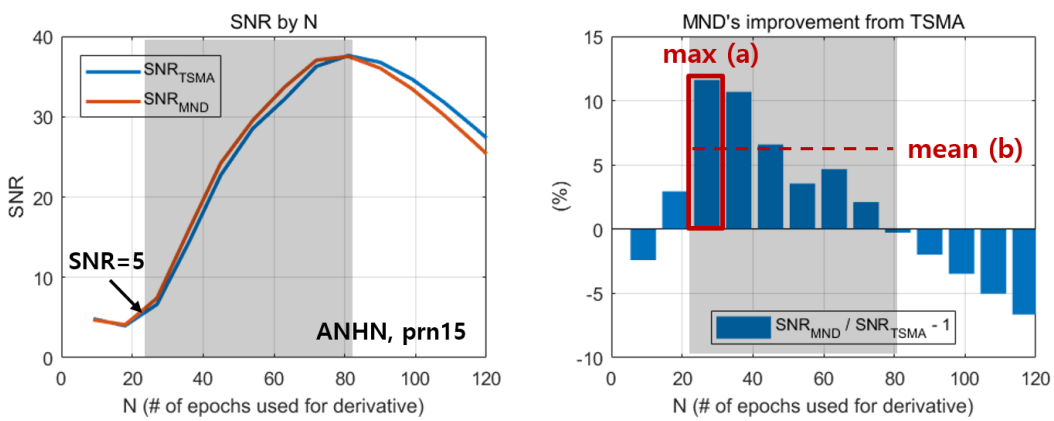

Figure III−17. SNR comparison of TSMA and MND in small N regions for early detection scenario

Table III-4. Improvement of MND from TSMA for small N regions

prn	max (a)	mean (b)
15	7.4 %	3.8 %
26	5.9 %	2.2 %
27	5.9 %	2.7 %

In conclusion, MND has better maximum SNR compared to Numerical 3rd order derivative, FDMA, and BP, and similar SNR with TSMA. However, when comparing SNR performance in small N regions related to early detection, MND shows better performance that TSMA.

V. Epicenter Estimation

1. Energy Propagation Mechanism

CID by Rayleigh wave is the first observed disturbance among ionospheric disturbances by earthquake. When the earthquake occurs, the Rayleigh wave spreads around the epicenter with a circular wave of about 3.5 km/s. At this time, the surface wave of the crust generates an acoustic wave moving vertically through coupling with the atmosphere. Since the acoustic waves generated by the Rayleigh wave arrive at the ionosphere sequentially, disturbances with a speed of 3.5 km/s are observed in the ionosphere. This is schematically shown in Figure V-1. There is a time difference of 10 minutes between the Rayleigh wave on the surface and CID above, which is the time it takes for the acoustic wave to reach from the surface to the ionosphere. The speed of the sound waves is 340 m/s on the surface but increases to 1 km/s due to the high temperature in the ionosphere, which means that the average speed is around 580 m/s up to a height of 350 km with a maximum electron density. This corresponds to the 10 min time offset.

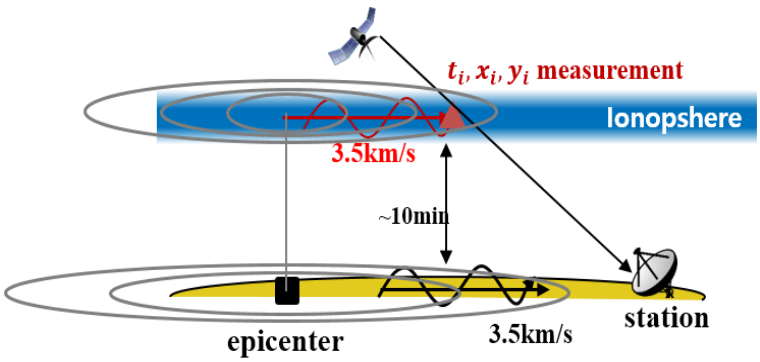

Figure V-1. CID by Rayleigh wave propagation

2. Epicenter Estimation Using CID Data

The proposed epicenter estimation method uses initial disturbance by Rayleigh wave. CID by Rayleigh is observed first because it has the fastest speed as mentioned above. In the case of the second arriving acoustic gravity wave, it is difficult to specify the starting point due to remaining disturbances by the Rayleigh wave. Therefore, the ionospheric disturbance point by Rayleigh wave is the most suitable data for position estimation. There are two kinds of information on the ionospheric disturbance obtained using the GNSS signal. The first is time information at the beginning of ionospheric disturbance, and the second is location information corresponding to the latitude and longitude of the ionospheric pierce point (IPP) at the disturbance point. This data is illustrated as red triangles as shown in Figure V-2.

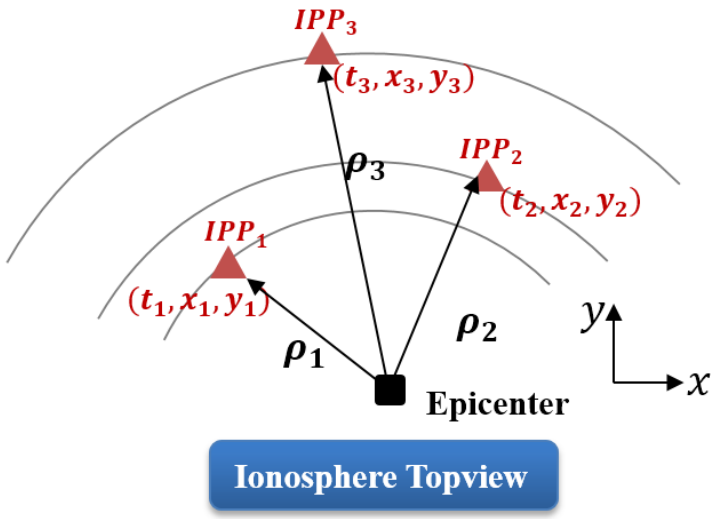

Figure V−2. CID data for epicenter estimation

For 2D propagation of CID, Equation (V.1) holds.

$$\rho_i = v_R(t_i - t_0) \qquad (V.1)$$

Here, v_R means the speed of Rayleigh wave, which is 3.5 km/s, t_i the time of CID detection, t_0 the starting time of CID above epicenter, and r_i the 2D distance from IPP_i and epicenter. ρ_i is calculated by latitude/longitude information of epicenter and IPP_i. Then we can express error as Equation (V.2).

$$e_i = (\rho_i - v_R t_i + v_R t_0)^2 \qquad (V.2)$$

Before explain the estimation process in detail, we will explain how to extract CID arrival time from the ionospheric time. MND 3rd derivative with N=100 is used for de-trending and reducing noise of the measurement.

It is difficult to accurately determine when the CID has arrived. This is because even when there is no disturbance, ionospheric combination has a noise component. Therefore, a standard that can be applied equally to all measurements is necessary. The method used in this study is to extract the first peak in the region of interest. The disturbance arrival time thus extracted has a time offset of the actual disturbance arrival time and a certain size, but it is acceptable because it is included in t_0 as a bias.

The region of interest refers to the time from 10 min to 20 min after the earthquake, 10 min to the arrival of the ionosphere disturbance just above the epicenter, and 20 min to the disturbance reaching the ionosphere 2000 km from the epicenter. Most of the disturbance disappears when the distance exceeds 2000km, so 20 min is selected as the upper boundary.

Before extracting time, MND 3rd order derivative result of ionospheric combination was normalized by noise modeling [20]. For this, all PRNs, and Korean GNSS stations DOND, WOLS, CHLW, KUNW, CHCN were used on the day of the Tohoku Earthquake. In order to eliminate the effect of CID on noise modeling, 6 hr long data

from the time of earthquake outbreak was removed. As shown in Figure V−3, noise increases with low elevation angle.

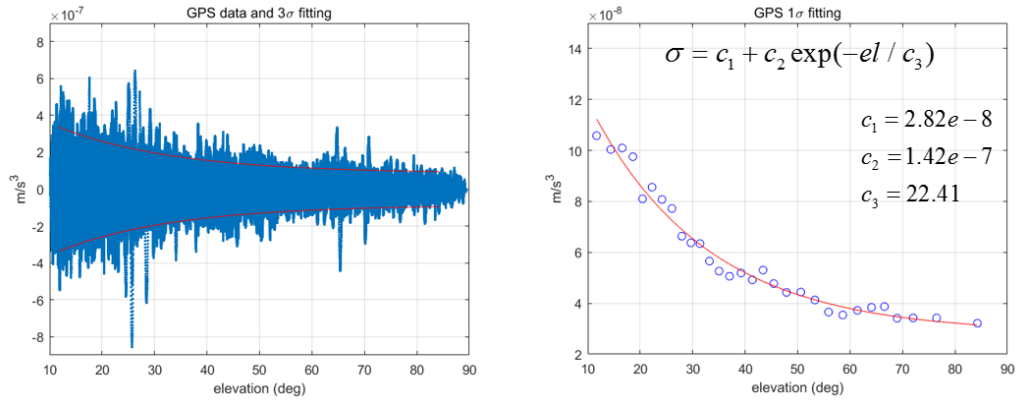

Figure V−3. Noise modeling of MND 3rd by elevation

Figure V−4 shows the extracted time of CID arrival. Here, MND 3rd order derivative of ionospheric combination was normalized by 1 sigma of noise model.

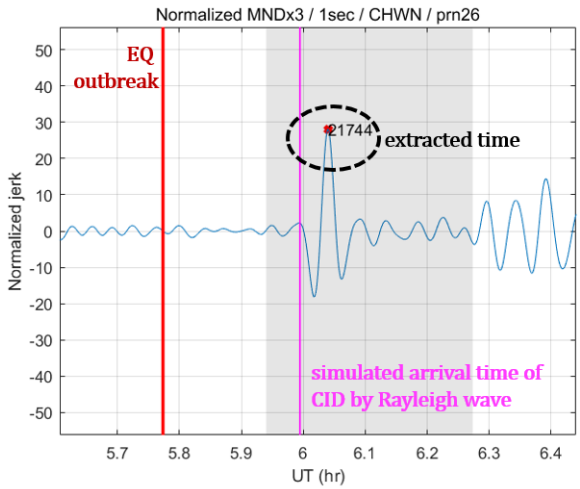

Figure V−4. CID arrival time extraction

The arrival time of CID by Rayleigh wave was extracted using a simple criterion; to select the first peak in the region of interest above normalized value 10. After extracting the arrival time data, bad data was removed manually. In this process, anomaly data due to missing epochs or abnormal shape of CID was eliminated, which improves the estimation.

As for the position data of IPP, the IPP latitude and longitude at the disturbance time are calculated based on the Klobuchar model, where the altitude of the thin shell is assumed to be 350 km.

$$J = \sum_{i=1}^{m} (\rho_i - v_R t_i + v_R t_0) \qquad (V.3)$$

After applying the cost described in Equation (V.3), the epicenter can be calculated by finding the point where the sum of cost is minimized. We used the MATLAB built-in function fmincon to calculate the solution. Here, estimated variables are three: the starting time of CID above epicenter t_0 and the location of earthquake in latitude and longitude $(\phi_{EQ}, \lambda_{EQ})$.

If the measurement is concentrated on either side only on the basis of the epicenter, this results in poor results in terms of DOP (Dilution Of Precision). In this study, we improved this by adding data of GUAM station. This improves the DOP, which results in more stable position estimation.

Table V-1. Data used for epicenter estimation

GNSS	sampling time	station	PRN
GPS	1 sec	NGII (50 stations in Korea)	5,15,26,27
		IGS (GUAM)	15,26,27

The epicenter estimation result is shown in Figure V-5 and Table V-2. In Figure V-5, each colored dot represents the IPP location at the time of CID detection. The color of the point represents the delay time until the initial disturbance is observed after the earthquake. The black triangle is an epicenter of an earthquake estimated by the United States Geological Survey (USGS), which is assumed to be true value. The distance error was calculated from this value.

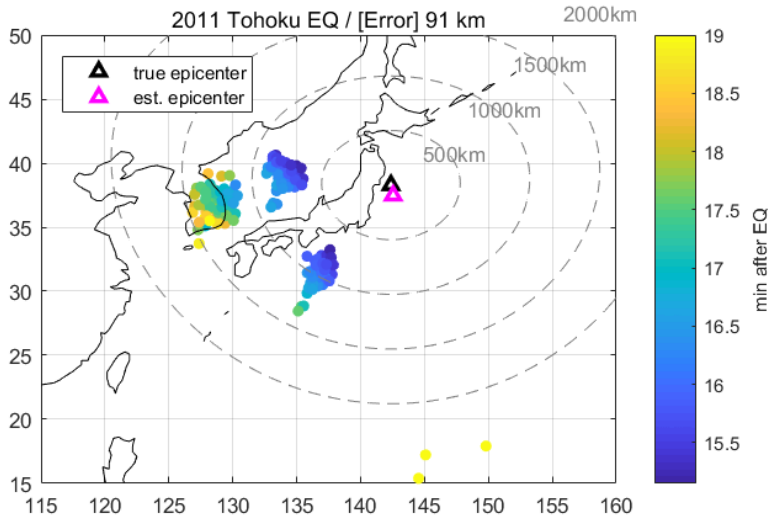

Figure V-5. Epicenter estimation result

Table V-2. Epicenter estimation result

	Latitude (deg)	Longitude (deg)	Error distance
True (USGS)	38.30°	142.37°	-
Previous study	37.50°	144.00°	170km
Proposed	38.49°	142.55°	91km

Each point in the graph represents the IPP location at the time of the initial disturbance observed by the Rayleigh wave. The color of the point represents the time until the initial disturbance is observed after the earthquake. From blue to yellow, the time from earthquake

to disturbance detection is long. Circles indicated by dashed lines represent concentric circles of 500 km from the estimated epicenter. Due to the nature of the spherical earth expressed on two dimensions of latitude and longitude, a circle with a certain degree of distorted shape is drawn. The black triangle is an epicenter of an earthquake estimated by the United States Geological Survey (USGS). In this study, the distance error was calculated from the true value.

Table V-2 shows the result of epicenter estimation, the distance error of proposed method was 91 km, which is 45% improved result from the previous study [16].

VI. **Conclusion**

In this study, a new time derivative method was introduced and analyzed. It can effectively detect disturbance of ionosphere due to earthquakes by reducing noise while preserving the disturbance signal.

We investigated the SNR for ionospheric disturbance detection, which was not performed previously. The designed algorithm, Minimum Noise Derivative (MND) that minimizes noise, confirmed that the SNR of the CID is maximized when one epoch slope is estimated using 100 epochs based on the Tohoku Earthquake data. Compared with the moving average and band-pass results, the performance improvement of 12% and 13% was observed, respectively. Also, in case of TSMA (Time Step & Moving Average), which performs moving average with expanded time interval of difference, it showed similar SNR with MND. However, SNR of MND is relatively higher than TSMA when small epoch is used. This means that MND performance is superior to TSMA in terms of fast detection & early warning.

In addition, we estimated the epicenter of the 2011 Tohoku earthquake using the Korean GNSS stations. The disturbance arrival time was calculated with the result of MND 3rd derivative. The propagation model of CID assumed 2D, with a constant Rayleigh wave velocity of 3.5 km/s. We obtained a position error of 91 km, which is 45% improved result over the previous study with 170 km.

Reference

[1]P. Lognonné, E. Clévédé, and H. Kanamori, "Computation of seismograms and atmospheric oscillations by normal-mode summation for a spherical earth model with realistic atmosphere," *Geophys. J. Int.*, vol. 135, no. 2, pp. 388–406, 1998.

[2]E. Calais, J. Bernard Minster, M. Hofton, and M. Hedlin, "Ionospheric signature of surface mine blasts from Global Positioning System measurements," *Geophys. J. Int.*, vol. 132, no. 1, pp. 191–202, 2002.

[3]C. Hines, "Atmospheric gravity waves:{A} new toy for the wave theorist," *Radio Sci.*, vol. 69, no. 3, pp. 375–380, 1965.

[4]K. Heki and J. Ping, "Directivity and apparent velocity of the coseismic ionospheric disturbances observed with a dense GPS array," *Earth Planet. Sci. Lett.*, vol. 236, no. 3–4, pp. 845–855, 2005.

[5]N. P. Perevalova, V. A. Sankov, E. I. Astafyeva, and A. S. Zhupityaeva, "Threshold magnitude for ionospheric response ionospheric TEC response to earthquakes," *J. Atmos. Solar-Terrestrial Phys.*, vol. 108, no. January, pp. 77–90, 2014.

[6]G. Occhipinti, L. Rolland, P. Lognonné, and S. Watada, "From Sumatra 2004 to Tohoku-Oki 2011: The systematic

GPS detection of the ionospheric signature induced by tsunamigenic earthquakes," *J. Geophys. Res. Sp. Phys.*, vol. 118, no. 6, pp. 3626–3636, 2013.

[7] S. Jin, G. Occhipinti, and R. Jin, "GNSS ionospheric seismology: Recent observation evidences and characteristics," *Earth-Science Rev.*, vol. 147, pp. 54–64, 2015.

[8] L. M. Rolland, P. Lognonné, and H. Munekane, "Detection and modeling of Rayleigh wave induced patterns in the ionosphere," *J. Geophys. Res. Sp. Phys.*, vol. 116, no. A5, pp. 1–18, 2011.

[9] J. Artru, V. Ducic, H. Kanamori, P. Lognonné, and M. Murakami, "Ionospheric detection of gravity waves induced by tsunamis," *Geophys. J. Int.*, vol. 160, no. 3, pp. 840–848, 2005.

[10] A. Komjathy *et al.*, "Detecting ionospheric TEC perturbations caused by natural hazards using a global network of GPS receivers: The Tohoku case study," *Earth, Planets Sp.*, vol. 64, no. 12, pp. 1287–1294, 2012.

[11] L. T. Xiahong Zhang, "Detection of ionospheric disturbances driven by the 2014 Chile tsunami using GPS total electron content in New Zealand," no. 1, pp. 5259–5271, 2014.

[12] M. Hernández-Pajares, J. M. Juan, and J. Sanz, "Medium-scale traveling ionospheric disturbances affecting GPS measurements: Spatial and temporal analysis," *J.*

Geophys. Res. Sp. Phys., vol. 111, no. 7, pp. 1–13, 2006.

[13] J. Park, D. A. Grejner-Brzezinska, R. R. B. Von Frese, and Y. Morton, "GPS discrimination of traveling ionospheric disturbances from underground nuclear explosions and earthquakes," *Navig. J. Inst. Navig.*, vol. 61, no. 2, pp. 125–134, 2014.

[14] J. Park, "Ionospheric Monitoring by the Global Navigation satellite system," vol. PhD, 2012.

[15] J. Park, R. R. B. Von Frese, D. A. Grejner-Brzezinska, Y. Morton, and L. R. Gaya-Pique, "Ionospheric detection of the 25 May 2009 North Korean underground nuclear test," *Geophys. Res. Lett.*, vol. 38, no. 22, pp. 1–6, 2011.

[16] T. Tsugawa *et al.*, "Ionospheric disturbances detected by GPS total electron content observation after the 2011 off the Pacific coast of Tohoku Earthquake," *Earth, Planets Sp.*, vol. 63, no. 7, pp. 875–879, 2011.

[17] Y. M. Yang *et al.*, "Tohoku-Oki earthquake caused major ionospheric disturbances at 450 km altitude over Alaska," *Radio Sci.*, vol. 49, no. 12, pp. 1206–1213, 2014.

[18] O. A. Godin, "Acoustic-gravity waves in atmospheric and oceanic waveguides," *J. Acoust. Soc. Am.*, vol. 132, no. 2, pp. 657–669, 2012.

[19] V. Ducic, J. Artru, and P. Lognonné, "Ionospheric remote sensing of the Denali Earthquake Rayleigh surface waves," *Geophys. Res. Lett.*, vol. 30, no. 18, pp. 1–4, 2003.

[20]B. Park, “A Study on Reducing Temporal and Spatial Decorrelation Effect in GNSS Augmentation System: Consideration of the Correction Message Standardization,” 2008.

초 록

지진으로 인한 에너지는 지표와 대기의 에너지 상호작용으로 인해 전리층으로 전달되어 Co-seismic Ionospheric Disturbance (CID)를 발생시킨다. CID는 L1, L2 반송파를 이용하여 추정한 전리층 지연을 통해 관측할 수 있다. 지진이 없는 정상상황에서 전리층 지연의 경향성은 일반적으로 교란보다 크므로, 전리층 지연에서 교란 신호를 분리하기 위해 band-pass, 미분법 등의 방법이 사용된다. 지진의 규모가 작거나 신호가 진원지에서 멀리 떨어진 경우 교란이 잡음에 묻혀 검출이 어려운 단점이 있다. 따라서 작은 교란을 효과적으로 검출하기 위해서는 교란의 신호 대 잡음비(SNR)를 높이는 것이 필수적이라 할 수 있다.

본 논문에서는 전리층 조합의 선형조합을 통해 잡음을 감소시키는 새로운 미분법을 제안하고, band-pass 및 기존의 미분법에 대해 잡음 수준, 최대 SNR, 초기경보 환경에서의 SNR을 비교하였다. 이때 실측데이터로는 2011년 도호쿠 지진 데이터를 활용하였다.

또한, CID 정보를 기반으로 진앙 위치 추정을 수행하였다. 이때 CID 검출 시간은 제안된 알고리즘을 사용하여 추출하였으며, 간단한 2D CID 전파 모델이 사용되었다. 이를 통해 도출한 진앙 위치 추정 성능을 선행연구와 비교하였다.

주요어: 전리층, 지진에 의한 전리층 교란 (CID), 지진, 신호 대 잡음비(SNR)

학 번: 2017-24591